

Intraslab Stresses in the Cascadia Subduction Zone from Inversion of Earthquake Focal Mechanisms

by Ikuko Wada,* Stéphane Mazzotti, and Kelin Wang

Abstract At the Cascadia subduction zone, intraslab earthquakes occur mostly in the northern part of the margin and its southern end, the Mendocino triple junction (MTJ). We determine intraslab stress orientations by inverting earthquake focal mechanisms and develop working hypotheses to explain the inferred intraslab stresses and observed seismicity. Our inversion results show that the subducting Juan de Fuca (JDF) slab in northern Cascadia is primarily under compression normal to the slab surface and tension in the downdip direction, most likely controlled by the net slab pull. An exception is a northernmost shallow region near the Nootka fault zone where the state of stress is dominated by nearly east–west tension. We hypothesize that the shear force on the Nootka fault zone and margin-parallel mantle resistance to slab motion induce the east–west tension in this region. Near the MTJ, stresses in the JDF plate are dominated by north–south compression down to about 20 km depth, consistent with a strong push by the Pacific plate from south of the Mendocino transform fault, but the deeper part of the slab shows downdip-tension, similar to northern Cascadia. Deviatoric stresses in the JDF slab appear to be very low, resulting in very low intraslab seismicity. In comparison with northern Cascadia, the stresses in most of southern Cascadia are even lower, resulting in nearly no intraslab seismicity.

Online Material: Earthquake focal mechanism data.

Introduction

At the Cascadia subduction zone, the young (4–11 Ma at the deformation front) Juan de Fuca (JDF) plate subducts obliquely beneath the North America plate at ~40 mm/yr (DeMets *et al.*, 1990, Wilson, 1993; DeMets *et al.*, 1994) (Fig. 1). Intraslab earthquakes occur in northern Cascadia to a maximum depth of ~90 km. Their occurrence is not as frequent as in most other subduction zones, but they are responsible for most of the earthquake-related damage in this region over the past century. The most recent damaging event of this type is the M_w 6.8 Nisqually earthquake of 2001. In contrast, intraslab earthquakes are nearly absent in southern Cascadia except near the Mendocino triple junction (MTJ). The intriguing along-strike variation in intraslab seismicity has been an outstanding issue in both geodynamics research and earthquake hazard analysis at this margin.

The occurrence of intraslab earthquakes appears to require both stresses and elevated pore fluid pressure. The former causes faults to fail, and the latter, which can be produced by thermally controlled slab dehydration, causes the

failure to be brittle and seismic (Kirby *et al.*, 1996; Hacker *et al.*, 2003). Dehydration of the slab at shallower depths due to the warmer state of the slab as a result of a slightly slower subduction rate has been proposed to explain the paucity of intraslab earthquakes in southern Cascadia (e.g., Wong, 2005). However, intraslab earthquakes occur in the northernmost part of Cascadia, where the slab is even warmer than in most of southern Cascadia because of its very young age (<6 Ma) (Wilson, 1988, 1993). Therefore, the primary cause of the along-strike variation in intraslab seismicity is unlikely to be a difference in the metamorphic state of the slab and is expected to be a difference in the state of stress.

The state of stress in the subducting slab can generally be inferred from focal mechanisms of intraslab earthquakes. In Cascadia, however, such inferences were previously made only in a few selected small areas. In this study, we compile existing and newly determined focal mechanism solutions for intraslab earthquakes from the entire Cascadia margin and apply a newly available inversion method to the solutions. We then propose some working hypotheses to explain the inferred intraslab stresses and the distribution of intraslab seismicity including the north–south contrast. Examining intraslab stresses from the whole-margin perspective, especially

*Now at Department of Geology and Geophysics, Woods Hole Oceanographic Institution, 266 Woods Hole Road, Woods Hole, Massachusetts 02543-1050.

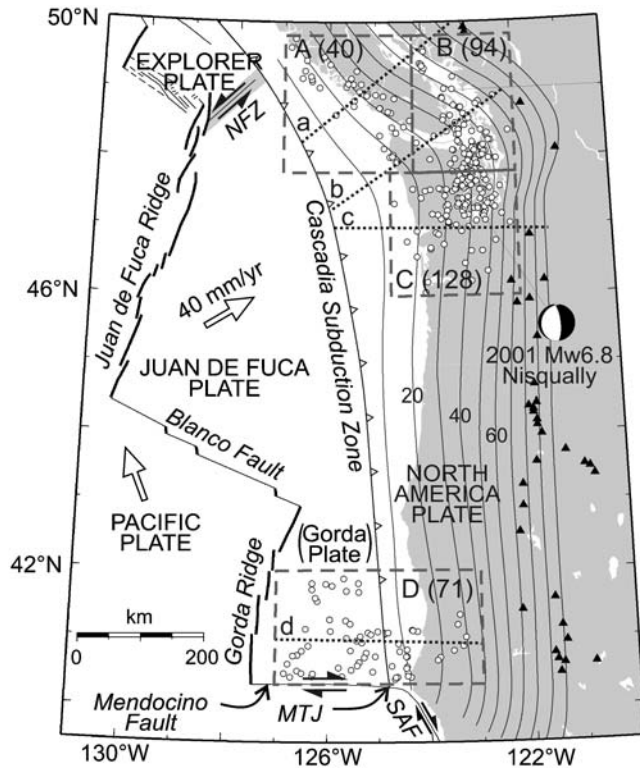


Figure 1. The Juan de Fuca (JDF) plate system. Hollow arrows indicate plate motions relative to North America (DeMets *et al.*, 1990; Wilson, 1993; DeMets *et al.*, 1994). The direction of the absolute motion of the JDF plate is similar to that relative to North America (Gripp and Gordon, 2002). NFZ: Nootka fault zone. MTJ: Mendocino triple junction. SAF: San Andreas fault. Solid triangles represent volcanic centers. Thin solid lines are slab surface contours of McCrory *et al.* (2004), with the depth indicated in kilometers. Stress orientations were determined for four regions, A, B, C, and D, bounded by dashed lines, by using earthquakes in the JDF plate shown by open circles. The number of events in each region is shown in parentheses. The dotted lines labeled as a, b, c, and d indicate the profile lines of cross-sections for regions A, B, C, and D, respectively, shown in Figure 2.

when linked to knowledge obtained by previous studies of the stress state of the unsubducted part of the JDF plate (e.g., Wang *et al.*, 1997), leads to a better understanding of the plate-scale geodynamics.

Determination of Stress Orientations

Stress Inversion Method

Several existing inversion algorithms estimate the orientations of the maximum, intermediate, and minimum principal stress axes: σ_1 , σ_2 , and σ_3 , respectively, and the stress magnitude ratio $R = (\sigma_1 - \sigma_2)/(\sigma_1 - \sigma_3)$, using a suite of focal mechanisms from a given source region. The fundamental concept embedded in all these methods is that σ_1 and σ_3 lie in the compressional and dilatational quadrants, respectively, of a focal mechanism (McKenzie, 1969). When there is little variation in the population of focal mechanisms, due possibly to a single prevailing orientation of preexisting

zones of weakness, the solution is not well constrained. Inverting very similar focal mechanisms is almost equivalent to inverting one focal mechanism. Therefore, diverse fault plane orientations are required. An important assumption made in the inversion is that the stress field is uniform over the source region spanned by the data set. The choice of the size of the source region thus needs to be carefully made.

Stress orientations determined by using different algorithms on the same data set are generally in good mutual agreement (e.g., Hardebeck and Hauksson, 2001). Two commonly used algorithms are the grid search inversion algorithm of Gephart and Forsyth (1984) and the linear inversion algorithm of Michael (1984, 1987). Gephart and Forsyth's (1984) method allows fault plane orientations to be adjusted within an error range during the inversion and selects a fault plane from the two nodal planes of each solution. However, when the method is tested with synthetic data sets, the confidence regions of the solutions are found to be too large (Hardebeck and Hauksson, 2001), and the R value may be poorly determined (Kastrop *et al.*, 2004). Michael's (1984, 1987) method assumes no errors in fault plane orientations and uses both nodal planes of the focal mechanisms. The confidence region of the solution is determined through statistical bootstrapping. It is reported to give better defined confidence regions and more reasonable R values (Hardebeck and Hauksson, 2001).

In the present study, we use the Bayesian parameter estimation method of Arnold and Townend (2007). In comparison with other algorithms, its advantages include the incorporation of uncertainties in the focal mechanism solutions, a statistical treatment of nodal plane ambiguity, and a weak constraint imposed on the stress tensor by a population of similar focal mechanisms in a suite. This method yields a joint 4-D *a posteriori* probability density function (PDF) of the three Euler angles (ϕ_s , θ_s , ψ_s) of the stress tensor and the R value. In this study, uniform probability distribution is assumed for the three Euler angles over their respective maximum possible ranges as *a priori* information, and a Matrix-Fisher distribution is assumed for errors in focal mechanism solutions. The results are illustrated by using a lower-hemisphere projection of contours of the marginal probability density of the three principal stress axes. The tightness of the contours depicts how well the stress orientation is constrained. The mean and the mode (i.e., the maximum value of a PDF) for each principal stress axis obtained from the 4-D PDF are also plotted on the projection. Arnold and Townend (2007) explain that large disagreement between the mode and the mean is indicative of the precision (i.e., the tightness of the contours) of the estimated stress orientations being not justified by the data. Two separate marginal *a posteriori* PDFs of the strike and the dip of each axis will also be plotted for some of our results.

Focal Mechanism Solutions

For the determination of intraslab stress orientations in northern Cascadia, we used both moment-tensor and

first-motion focal mechanism solutions that had been determined by various research groups (Fig. 1). The moment-tensor solutions consist of those determined by Ristau (2004) and H. Kao (2008, personal communication) for eight intraslab events during 1994–2003 and those determined by the Oregon State University for five events during 1994–1998 (see the [Data and Resources](#) section). These solutions are for events of $M \geq 3.8$ except for two smaller ones (M 2.9 and 3.5) determined by H. Kao (2008, personal communication). The first-motion focal solutions are primarily for smaller earthquakes and consist of 40 solutions of Ma *et al.* (1996) for events during 1980–1985, 163 of the Pacific Northwest Seismograph Network (PNSN) for events during 1972–2007 (see the [Data and Resources](#) section), and 28 of Bolton (2003) for events during 1985–2001. The PNSN quality level ranges from 0 for the best quality to 1 for the worst quality. We used those with quality values no greater than 0.1. Those PNSN solutions that overlapped with the 13 moment-tensor solutions were excluded. If two or more first-motion solutions were available for the same event, we kept one solution in the order of precedence of Ma *et al.* (1996), PNSN, and Bolton (2003). The PNSN and Bolton (2003) solutions were obtained as part of the routine processing of seismic-network data, but the solutions by Ma *et al.* (1996) went through a more rigorous research process.

We augmented the northern Cascadia data set by determining first-motion focal mechanism solutions for other intraslab earthquakes recorded by the Canadian National Seismic-Network during 2003–2006. We used the FPFIT program (Reasenberg and Oppenheimer, 1985), which is a widely used program to determine focal mechanisms from P -wave first-motion polarity data through grid search inversion. Out of 24 events with sufficient station coverage, 18 of them yielded convergent and well-constrained solutions. Including the 18 newly determined solutions, the total number of focal mechanism solutions in our northern Cascadia data set is 272. For the 272 focal mechanism data, [E](#) see Table E1 in the electronic supplement to this article.

There is little intraslab seismicity in southern Cascadia except near the MTJ. For the determination of intraslab stress orientations near the MTJ, we used the 71 focal mechanism solutions provided by the National Earthquake Information Center (NEIC), U.S. Geological Survey (see the [Data and Resources](#) section, and [E](#) Table E2 in the electronic supplement to this article). The MTJ data set includes many events in the JDF plate seaward as well as landward of the deformation front, allowing a comparison of intraplate stresses before and after subduction. This is in contrast with northern Cascadia, where few earthquakes occur in the JDF plate prior to subduction although numerous events occur along its northern edge, the Nootka Fault Zone (NFZ), and in the Explorer plate farther north (Fig. 1).

For the inversion, we divided the northern Cascadia subduction zone into three regions, A, B, and C, in accordance with the strike and dip of the subducting JDF slab and called the MTJ area region D (Fig. 1). The number of focal mech-

anism solutions used in each region is shown in Figure 1, and the cross-sectional view of event distribution in each region is shown in Figure 2. None of the events we use are interplate earthquakes. Most of the events are much deeper than the seismogenic depth of the Cascadia megathrust (Fig. 2), and none of the shallow ones shows a thrust mechanism.

The Bayesian inversion approach employed in this work requires the uncertainties in the focal mechanism data to be collectively specified using an average value. The uncertainty value controls the preciseness of the fit of the inversion to the focal mechanism solutions. Uncertainties are not always specified for individual focal mechanism solutions from Cascadia, and we cannot readily derive an average uncertainty from these data. Through numerical testing, Arnold and Townend (2007) found it appropriate to use an average uncertainty of 20° in the strike, dip, and rake of the focal mechanism solutions for the type of *a priori* information on the unknown stress tensors explained in the preceding section. They showed that an uncertainty of 10° would overemphasize the data fit and produce unreasonable results for the stresses. Most of the focal mechanisms we use are first-motion solutions derived in the same way as those used by Arnold and Townend (2007). Therefore, one logical option

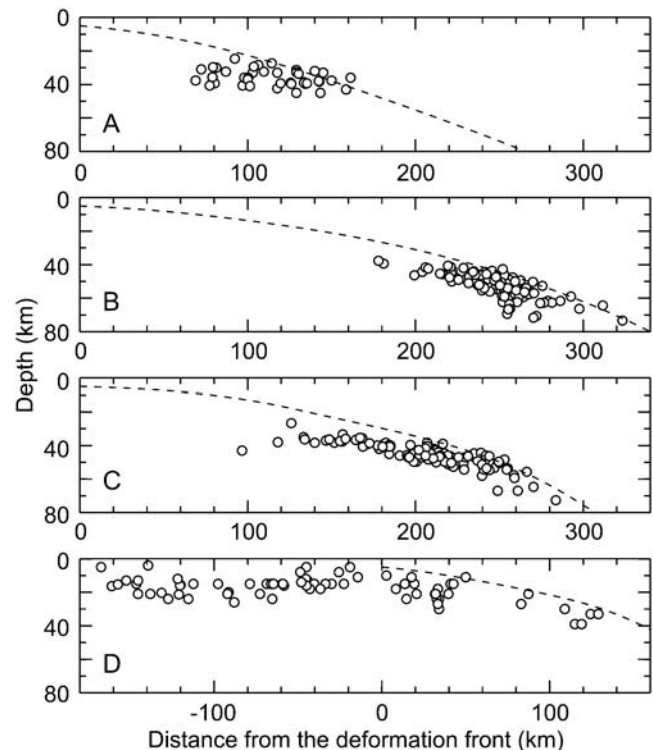


Figure 2. Cross-sections along-strike-normal profile lines, a, b, c, and d, shown in Figure 1 for region A, B, C, and D, respectively, showing the distribution of intraslab earthquakes (open circles) within each region used in the present study. A dashed line indicates the slab surface of McCrory *et al.* (2004) along the respective profile line. The shape of the slab surface slightly varies along-strike within each region; therefore, the hypocenters of some intraslab earthquakes are projected slightly above the dashed line.

for the present study is to follow [Arnold and Townend \(2007\)](#) and use an uncertainty of 20° .

Because there are relatively few intraslab earthquakes in Cascadia compared with most other subduction zones, we cannot afford to be too restrictive in selecting events for our stress inversion. This is the reason why we have included some small events from the routine-processing results given by the PNSN catalog and [Bolton \(2003\)](#). To provide a qualitative assessment of the quality of the routine-processing solutions, we compare the 39 events in our compilation for which focal mechanism solutions were given by both PNSN and a different research team (Fig. 3). The solutions shown in Figure 3b are used for our inversion; the PNSN solutions in Figure 3a are not used, but are displayed here for the purpose of comparison (for focal mechanism data, see [Table E3](#) in the electronic supplement to this article). A visual inspection of Figure 3 shows that although the two solutions agree for most of the events, there is significant disagreement for some of these events. We attribute the disagreement to errors in the PNSN solutions and assume that errors in the solutions by [Bolton \(2003\)](#) are at least at this level. To account for the potentially larger errors in the routine-processing solutions, we decided to invert the Cascadia data using a more conservative uncertainty of 30° as well as the 20° value recommended by [Arnold and Townend \(2007\)](#). However, it will be shown in the following section that the inversion results do not strongly depend on which of the two uncertainty values is used.

Inversion Results

We first present results for the three regions in northern Cascadia. The lower-hemisphere projection of the compressional (P) and tensional (T) axes of focal mechanisms for the three regions are shown in the first two columns of Figure 4.

For each region, we inverted the focal mechanism solutions assuming 20° and 30° uncertainties. The results, also shown in Figure 4, indicate that the two uncertainty assumptions yield similar stress orientations and R values. The contours are more spread out if a 30° uncertainty is assumed, reflecting the lower precision of the data. With either the 20° or 30° uncertainty, the mean and mode of the probability distribution for each axis are in close agreement within each region, although the agreement for region A is slightly worse if a 20° uncertainty is assumed. The results indicate that the stress orientations are well defined and the precision of their probability distributions well justified by the data with either uncertainty. Discussion in the rest of this paper will be based on results obtained with the 20° uncertainty.

Although discussions in this paper are based on results obtained using the Bayesian inversion method, we inverted the same data for the three northern regions also using [Michael's \(1984, 1987\)](#) linear inversion method in order to offer a comparison of our results with those by a more commonly used method. For the three regions, the stress orientations determined with the Bayesian inversion method are consis-

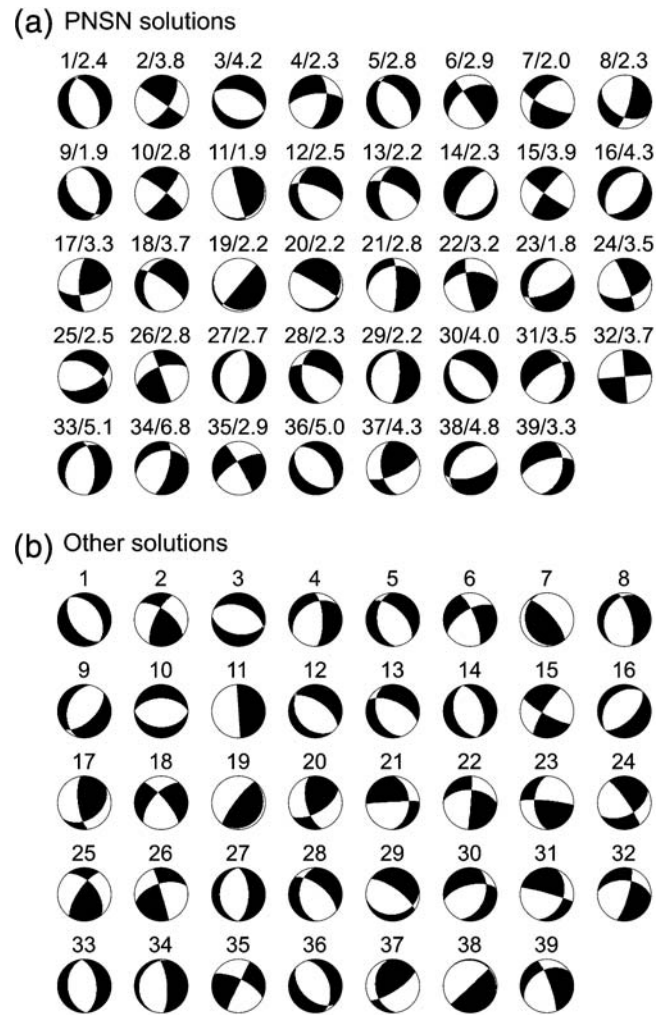


Figure 3. Comparisons of focal mechanisms provided by PNSN and other research teams for the 39 events for which both PNSN and non-PNSN solutions are available. (a) PNSN solutions. Each solution is labeled with the event number for this comparison and event magnitude. For focal mechanism data, see [Table E3](#) in the electronic supplement to this article. (b) Non-PNSN solutions. These solutions were used in our stress inversion, and the data are included in [Table E1](#) in the electronic supplement. Events 1–29 are the first-motion solutions by [Ma et al. \(1996\)](#); events 30–32 are the moment-tensor solutions by the Oregon State University; events 33–38 are the moment-tensor solutions by [Ristau \(2004\)](#); and event 39 is the first-motion solution determined in the present study.

tent with those determined with Michael's method (Fig. 4). The use of both nodal planes in Michael's method may result in greater uncertainties, but the 95% confidence regions determined by Michael's method are comparable to the 95% confidence intervals of the marginal PDFs of the azimuth and plunge of each stress axis shown in Figure 5. The R values determined by the two methods differ by up to 0.34 (region C), indicating the limitation of one or both of the methods in determining the R value. Inconsistent R values determined by different inversion methods were also noted in other studies (e.g., [Hardebeck and Hauksson, 2001](#); [Kastrup et al., 2004](#)). In the case of a large difference

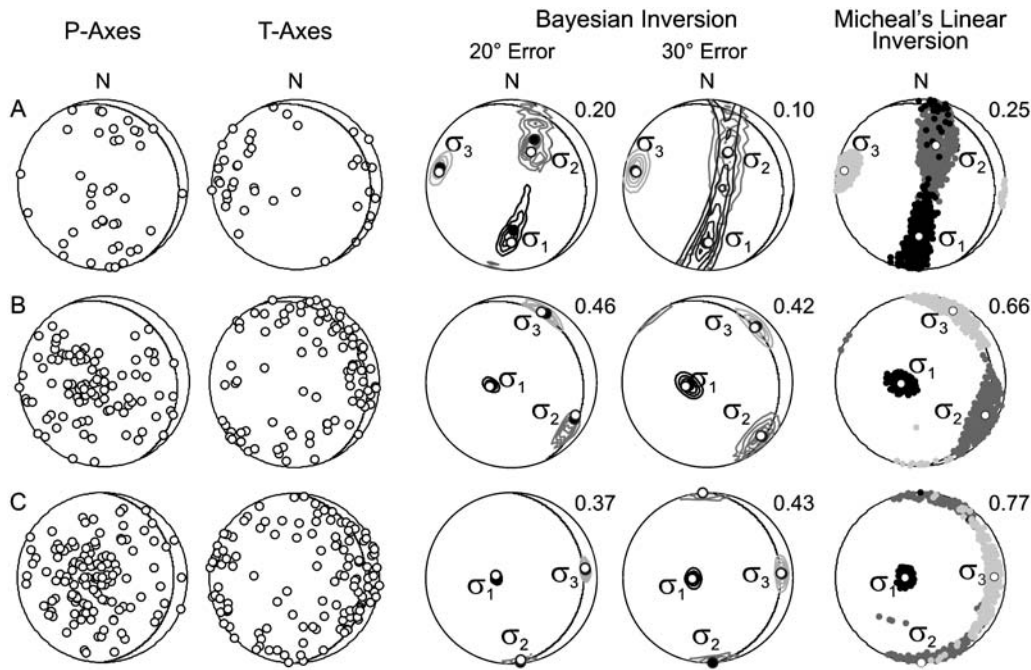


Figure 4. Focal mechanisms (lower-hemisphere equal-area projection) and inversion results for regions A, B, and C (Fig. 1). A great circle on each stereonet represents the average slab orientation in the region. For the Bayesian inversion results, assuming either 20° or 30° angular uncertainties in the focal mechanism solutions, black, dark gray, and light gray contours are marginal *a posteriori* probability density contours of the σ_1 , σ_2 , and σ_3 orientations, respectively. The open and filled circles are the mode and mean, respectively, of the three axes obtained from the 4-D PDF. See Figure 5 for the marginal *a posteriori* PDF of the azimuth and plunge of the three axes. For results obtained using Michael's (1984, 1987) linear inversion method, clouds of black, dark gray, and light gray dots correspond to the 95% confidence regions from bootstrapping for σ_1 , σ_2 , and σ_3 , respectively. The R value for each inversion result is shown to the upper right of the stereonet.

between the R values determined by the Bayesian and Michael's methods, we limit our discussion to stress orientations only.

In region A, the orientation of σ_3 is nearly east–west (Fig. 4), similar to the results of Bolton (2003), who used Michael's method with a smaller set of focal mechanism solutions. The σ_1 and σ_2 orientations are poorly defined, as shown by their widely spread contours in Figure 4 and the broad marginal PDFs of their azimuths and plunges in Figure 5. The relatively small R value of 0.1–0.2 indicates that the two stresses are very similar in magnitude and much larger than σ_3 . The elongated shape and the overlap of the probability density contours of σ_1 and σ_2 also indicate that they have almost the same magnitude.

In regions B and C, all of the three principal axes are relatively well defined. The results for region C are consistent with those of Ma *et al.* (1996) for the Puget Sound area. The most striking characteristic of the results is that the principal stresses are either normal to or parallel with the slab, indicating that slab-parallel shear stresses are very small. The marginal PDF for the azimuth of the slab-normal σ_1 is spread out widely in both regions (Fig. 5). This is due to its near-vertical plunge, which makes it difficult to resolve the azimuth. The direction of the least compressive stress σ_3 for both regions is approximately downdip.

To check if the assumption of a uniform stress field is valid for each region, we divided each region into smaller

subregions and inverted the focal mechanisms within each subregion (Fig. 6). Dividing regions A and C does not change the inversion results significantly, validating the assumption of uniform stress in these regions. The east–west σ_3 orientation in region A and the downdip σ_3 orientation in region C remain robust. In region B, the two subregions show different stress orientations (Fig. 6), but the orientations of σ_2 and σ_3 determined for region B as a whole (Fig. 4) are about an average of the corresponding axes determined for the two subregions (Fig. 6). This indicates that the two slab-parallel principal stresses σ_2 and σ_3 are similar in magnitude. Therefore, the assumption of uniform stress is also a reasonable one for region B, although possible small variations may be averaged out.

In the southern end of the margin, most intraslab earthquakes occur near the MTJ (in region D in Fig. 1). After a number of test runs, we found that using the three subregions as shown in Figure 7a best illustrates the state of stress and its spatial variations in this region. In both subregions D1 and D2, σ_1 is oriented north–south while σ_3 is east–west (Fig. 7b), consistent with the stresses predicted by Wang *et al.* (1997) using a model involving a transform push (to be further discussed in the Transform Push and North–South Compression Near the MTJ section) for the southernmost part of the JDF plate. Inverting the focal mechanism solutions from subregions D1 and D2 together would yield the same results, but separating them more clearly shows that the

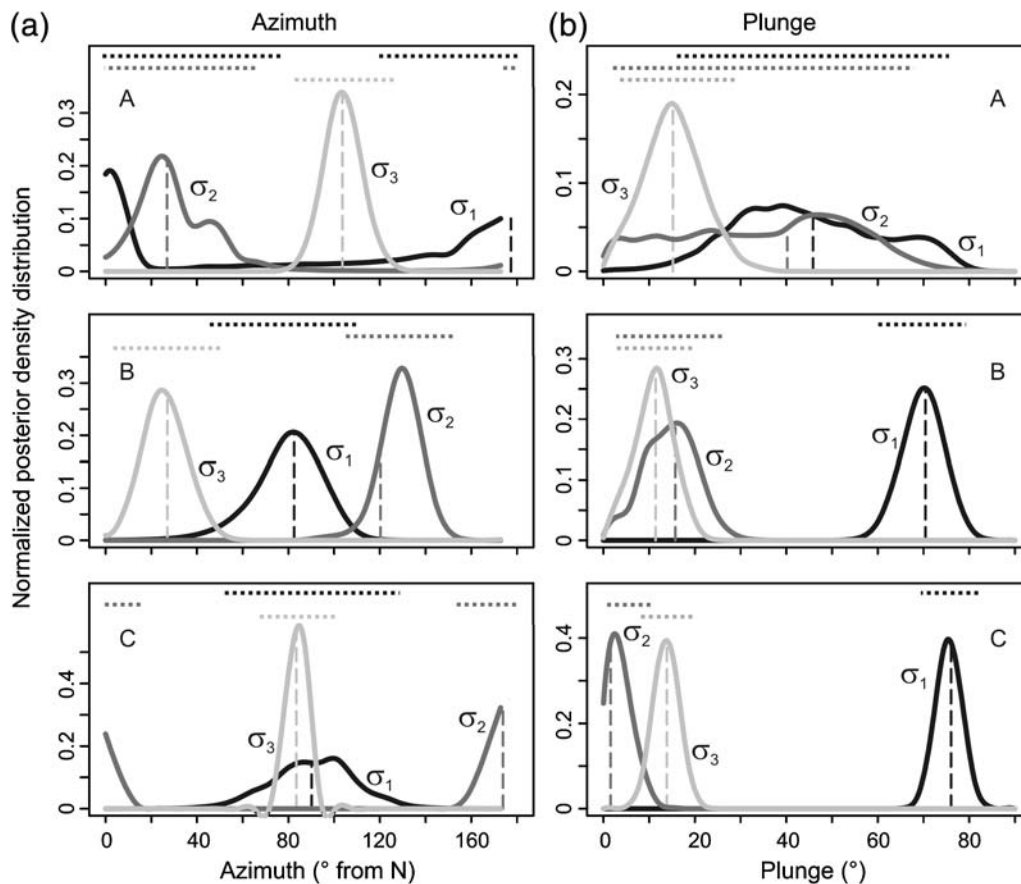


Figure 5. The marginal *a posteriori* PDF of (a) the azimuth and (b) the plunge of the principal stresses determined for regions A, B, and C by assuming a 20° focal mechanism uncertainty. The peak value of each distribution is the mode of the marginal *a posteriori* PDF; the vertical dashed line indicates the mean of the 4-D *a posteriori* PDF. They correspond to the open and solid circles, respectively, in the third column of Figure 4. The 95% confidence intervals for the three axes are shown using a dotted horizontal line over the peak of each curve.

effect of the transform push is present both before and immediately after subduction. However, in subregion D3, downdip from region D2 and away from MTJ, the orientation of σ_1 changes to slab-normal (Fig. 7b), similar to regions B and C in northern Cascadia.

Discussion

Here we attempt to identify forces that are responsible for the inferred intraslab stresses in northern Cascadia and near the MTJ. In the following discussion, compression or tension is relative to the lithostatic state. Because the shear stress on the plate interface (of the order of 10^0 – 10^2 MPa) (e.g., Wang and He, 1999; Lamb, 2006) is very small when compared with the lithostatic stress (10^3 – 10^4 MPa), the slab-normal stress takes nearly the lithostatic value. Therefore, a slab-parallel stress is either tensile or compressive, depending on whether it is less or greater, respectively, than the slab-normal stress.

Net Slab Pull and Downdip-Tension

In all regions except in region A and the shallow part of region D, the inferred orientation of σ_3 is predominantly

downdip. Slab pull, a primary driving force of plate subduction, is partly and locally balanced by resistance to subduction along the top and bottom of the subducting plate, but the leftover portion of slab pull, referred to as the net slab pull, induces downdip-tension in the slab (Fig. 8). Through geodynamic modeling, Schellart (2004) and Sandiford *et al.* (2005) show that the net slab pull is only about 10% of the total negative buoyancy of the slab. This net slab pull is most likely to be the cause for the inferred downdip-tension in northern and southernmost Cascadia.

In northern Cascadia, basalt-eclogite transformation in the subducting crust is predicted to occur at ~ 40 km depth (Wada *et al.*, 2008). The transformation causes a large (up to 15%) volume reduction, inducing an equivalent stretch in all slab-parallel directions within the subducting crust, because the overlying and underlying rocks do not experience the same volume reduction (Kirby *et al.*, 1996). Dehydration of hydrated mantle (serpentinite) along fractures may cause seismic failure (Kao *et al.*, 2008), but it does not take place until the slab reaches 80–90 km depths (Hacker *et al.*, 2003; Wada *et al.*, 2008) and is not expected to cause significant volume reduction at the slab scale (Wang, Cassidy, *et al.*, 2004). The result that the slab tends to be in tension in

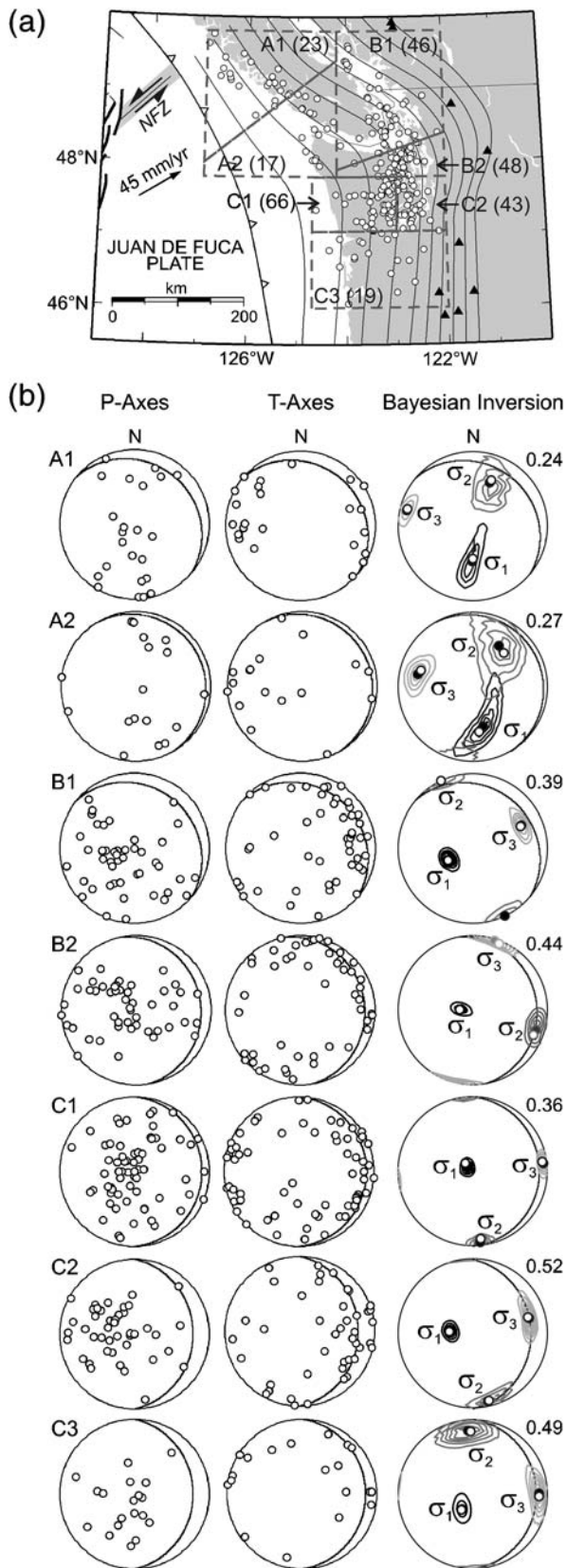


Figure 6. (a) Regions A, B, and C shown in Figure 1, divided into subregions. (b) Focal mechanisms and inversion results for the subregions. In all cases, a 20° uncertainty is assumed for the focal mechanisms. See Figure 4 for the explanation of symbols.

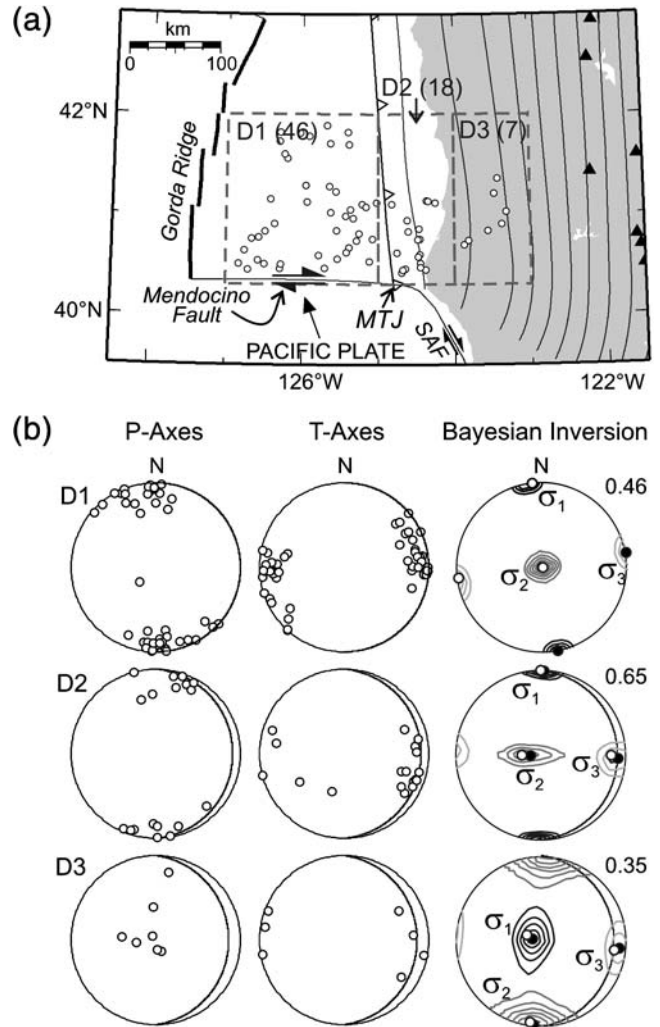


Figure 7. (a) Region D shown in Figure 1 divided into three subregions. (b) Focal mechanisms and inversion results for the subregions. In all cases, a 20° angular uncertainty is assumed for the focal mechanisms. See Figure 4 for the explanation of symbols.

the strike as well as downdip directions may imply that metamorphically induced slab-parallel stretch is taking place in the subducting crust. However, because in our study area earthquakes occur also in the subducting mantle that is not expected to experience metamorphically induced slab-parallel stretch (Cassidy and Waldhauser, 2003; Bolton, 2003; Medema *et al.*, 2004) and because the tension tends to be slightly greater in the downdip direction, the net slab pull appears to be a more dominant process controlling intraslab stresses at Cascadia.

In comparison, the role of the subduction zone interface and overriding plate in generating stresses in the JDFP and slab may be minor. The shear stress along the plate interface, included as part of the margin-normal slab resistance, has been shown to be very small (Wang and He, 1999). The seismogenic part of the interface is presently locked, and numerous geodetic observations indicate that the state of locking is rather uniform along-strike (Wang *et al.*, 2003; McCaffrey

et al., 2007). There is no evidence in these geodetic observations and in the stress inversion results presented here for significant along-strike variations of intraslab stresses due to heterogeneous locking of the seismogenic zone.

Bending of the slab, that is, an increase in the curvature of the slab in the downdip direction, should increase downdip-tension in the upper part of the slab, but this effect appears to be small at Cascadia because some of the downdip-tension earthquakes occur where the curvature of slab is no longer increasing or is even decreasing in the downdip direction (Fig. 2). The reason for the effect of bending to be small is perhaps the small thickness of the warm JDF slab. For the same curvature change, a greater bending stress will be induced in an older and thicker slab.

In subregion B2, where the arching of the slab is most prominent, the inferred orientation of σ_3 is arguably between downdip and margin-parallel. As discussed earlier, the readiness of the change in the orientations of the slab-parallel σ_2 and σ_3 over short distances within region B indicates that they must be similar in magnitude, allowing their orientations to be affected by other processes such as slab arching. The slab in a concave seaward subduction zone corner, as in the case of northern Cascadia, in theory experiences a margin-parallel compressive membrane stress (Chiao and Creager, 2002). However, the compressive stress (σ_1) in northern Cascadia as determined from earthquake focal mechanisms is primarily in the slab-normal direction. If the compressive membrane stress is indeed present, it must be overshadowed by other processes. Other proposed or speculated deformation processes, such as a ramp-flat-ramp slab geometry in the southern part of region B (Calvert, 2004) and a slab tear in region C (McCrorry *et al.*, 2004), may also affect intraslab stresses locally, although we do not see strong evidence for them.

Nootka Shear and Strike-Parallel Mantle Resistance to Slab Motion

The previously discussed tectonic processes do not explain the east–west orientation of σ_3 in region A, the northernmost and relatively shallow part of the JDF slab. We propose that the tension results from the combined effect of mantle resistance to slab motion and shear force along the Nootka fault zone (NFZ) at the northern boundary of the JDF plate (Fig. 8). The direction of the absolute motion of the JDF plate relative to the mantle is similar to its relative motion with respect to North America (Figs. 1 and 8). The obliquely subducting JDF slab experiences a mantle resistance in both the updip and south directions. Much of the updip component is locally balanced by the downdip slab pull, but the southern component is not balanced by a body force and hence induces a clockwise torque on the JDF plate (Wang *et al.*, 1997). The northwest-moving Pacific plate exerts fault-normal compression and a small right-lateral shear force along the Mendocino and Blanco transform faults (Fig. 1). These forces add to the clockwise torque.

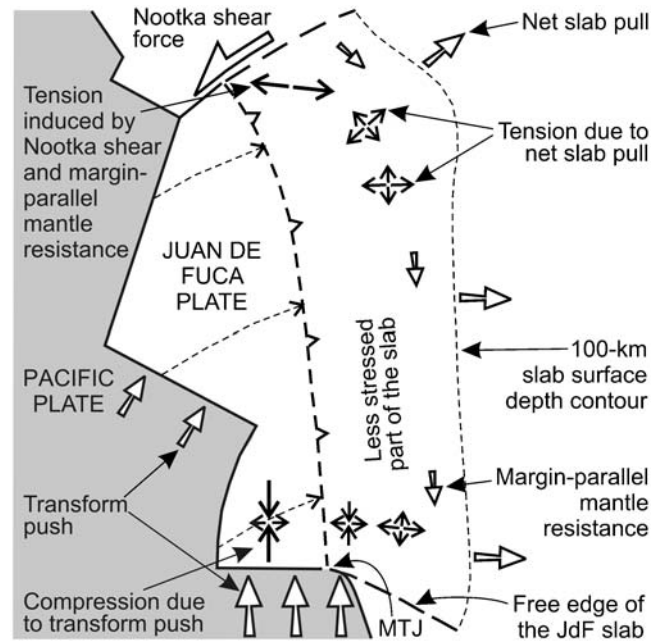


Figure 8. Diagram illustrating intraslab stresses (opposing or diverging arrows) and forces (white arrows) acting on the JDF plate. Thin dashed lines with an arrowhead on the incoming plate are approximate trajectories of absolute plate motion, indicating clockwise block rotation with a pole of rotation in the Pacific hotspot reference frame of Gripp and Gordon (2002) at 39°S 62°E.

This torque must be balanced by a counterclockwise torque, otherwise the clockwise rotation of the JDF plate around its center of mass would accelerate. There are three obvious candidates that may generate a counterclockwise torque: a northerly increase in margin-normal resistance to slab subduction, a northerly decrease in the slab pull, and a significant left-lateral shear force on the NFZ. The faster and less oblique motion of the slab relative to the absolute mantle reference frame in the north (Fig. 8) may result in a slightly greater margin-normal mantle resistance to subduction. In a model of the stress state of the JDF plate prior to subduction, Wang *et al.* (1997) showed that this may serve to balance the clockwise torque (their model V2), but they likely underestimated the clockwise torque because most of the subducted slab was not included in their model. Because the stress inversion results show downdip-tension in the north (Fig. 4, regions B and C) as well as in the south (Fig. 7), there is no compelling evidence for the slab pull to be much smaller in the north, although this possibility cannot be excluded. Regardless of the potential contributions from the along-strike variations in slab resistance and slab pull, we argue that the left-lateral shear force on the NFZ likely plays an important role in balancing the torque.

The NFZ developed as the Explore plate to the north was broken off from the JDF plate about 4 Ma ago (Riddihough, 1984). It is a broad shear zone characterized by frequent occurrence of moderate-size earthquakes (up to M 6.8) of similar strike-slip mechanisms (Fig. 9) and accommodates

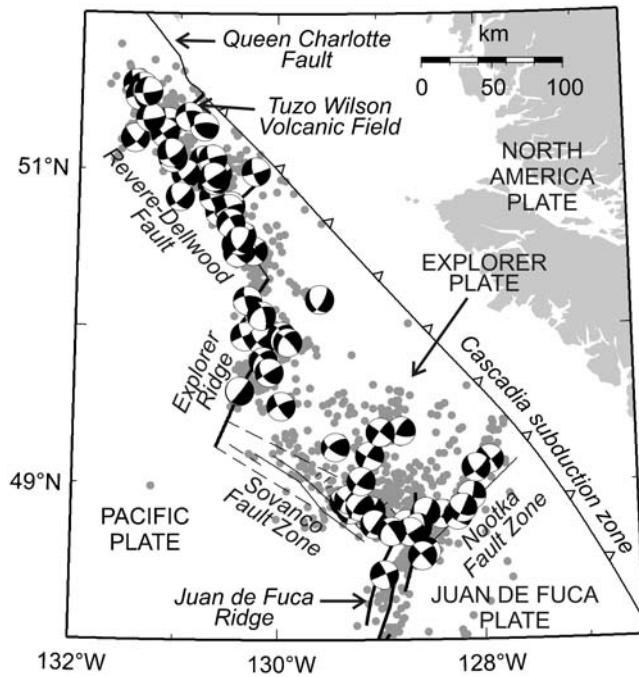


Figure 9. Earthquakes in the Nootka fault zone and Explorer plate area. Beach balls are moment-tensor solutions for earthquakes greater than magnitude 4.5 during 1995–2008 (see the [Data and Resources](#) section). Gray dots are other earthquakes ($M > 3$) during the same period.

at least 20 mm/yr of left-lateral shear ([Riddiough, 1984](#)). The orientation of the NFZ is highly oblique to the spreading ridge, and due to its unstable configuration, new faults must be created as the spreading at the ridge continues. Therefore, unlike transform faults such as the Mendocino fault that are weak in shear, the NFZ accommodates a large shear force. This NFZ shear can induce a counterclockwise torque on the JDF plate to balance the clockwise torque discussed previously. [Wang et al. \(1997\)](#) have shown that other forces such as ridge slide (also known as ridge push) and basal drag (viscous resistance on the base of the JDF plate) are less important in controlling stresses in the JDF plate.

The NFZ shear also affects the deformation of the Explorer plate northwest of the NFZ. Focal mechanisms of earthquakes within the Explorer plate are similar to those along the NFZ (Fig. 9). These earthquakes appear to represent right-lateral motion of strike-slip faults that are oriented almost perpendicular to the NFZ. These faults are probably modern or reactivated transform faults offsetting the Explorer ridge that forms the northwestern boundary of the Explorer plate. Different from the Gorda region, the Explorer plate mechanically is no longer a part of the JDF plate. Its kinematics are still under debate. According to a widely accepted model ([Riddiough, 1984](#); [Riddiough and Hyndman, 1989](#)), it is moving more or less coherently with respect to North America at about half of the rate of the JDF plate. According to a later proposed model ([Rohr and Furlong, 1995](#)), the Explorer plate no longer exists, with a part of it

captured by the North America plate and the rest by the Pacific plate. [Rohr and Furlong \(1995\)](#) proposed that a north-northwest trending right-lateral fault dividing the Pacific and North America plates has formed from the intersect of the NFZ and JDF ridge to the Tuzo Wilson volcanic field. The modern seismicity and focal mechanisms (Fig. 9) appear to be more consistent with the widely accepted model (see also [Braunmiller and Nábělek, 2002](#)), but the ongoing debate certainly reflects the complexity of this area.

Transform Push and North–South Compression Near the MTJ

Near the MTJ, the JDF plate prior to and just after subduction (subregions D1 and D2) is under north–south compression. The compression is obviously caused by the northward-moving Pacific plate pushing against the JDF plate, balancing mainly the margin-parallel slab resistance acting on the slab (Fig. 10). This push by the Pacific plate across the Mendocino transform fault is referred to as the transform push ([Wang et al., 1997](#)). The margin-parallel mantle resistance integrates along-strike, such that the north–south compression is the greatest at the southern end of the JDF plate ([Wang et al., 1997](#)). However, as suggested by [Wang and Rogers \(1994\)](#), strong compression is present only before and right after the plate starts to subduct. The deeper part of the slab is free of this effect because there is no longer a plate to provide transform push from the south. The absence of the transform push to balance the southerly mantle resistance to slab motion has important implications to slab deformation beneath northern California, impacting the debate on whether there is a stretched slab or a slab gap in the wake of the northward motion of the southern edge of the JDF plate ([ten Brink et al., 1999](#)). According to the results shown in Figure 7c, the deeper part of the slab is similar to most of the northern Cascadia, in a slab-pull-dominated state of downdip-tension and slab-normal compression.

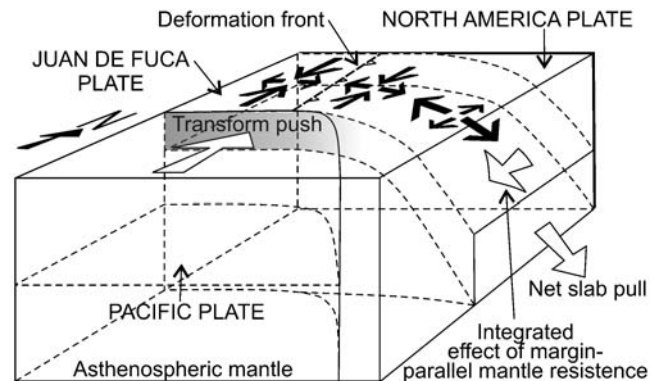


Figure 10. Diagram showing the tectonic structure of the Mendocino triple junction area and in-plate deviatoric stresses (thick black arrows) in the southernmost JDF plate. White arrows are forces acting on the plate.

North–South Contrast in Slab Seismicity

The near absence of intraslab seismicity in most of southern Cascadia is still a mystery. There does not seem to be a drastic difference in the metamorphic states of the subducting slab between northern and southern Cascadia as we discussed in the [Introduction](#). Therefore, we are forced to conclude that the slab in southern Cascadia is less stressed. In this section, we propose that the seemingly drastic north–south contrast in seismicity is caused by a small difference in deviatoric stresses.

There was early speculation that the deeper slab might be detached in parts of southern Cascadia, resulting in a nearly zero net slab pull ([Michaelson and Weaver, 1986](#)), but the presence of a subducting slab has been imaged to ~80 km depth in more recent studies (e.g., [Rondenay et al., 2008](#)). The results of a very large-scale seismic tomography feature a slab penetrating to much greater depths but with some apparent holes ([Sigloch et al., 2008](#)). However, [Roth et al. \(2008\)](#) show that at least an apparent hole beneath Oregon is an inversion artifact. We think that the net slab pull can be very small even without slab detachment if the slab is young and warm. A null or even negative net slab pull has indeed been inferred for the similarly warm subducting slab at the Nankai subduction zone ([Wang, Wada, and Ishikawa, 2004](#)).

The relatively simple state of stress in regions B, C, and D3 allows us to speculate on the magnitude of the slab pull and mantle resistance in Cascadia. The fact that one principal stress, in this case σ_1 , is normal to the slab in those regions is a statement that the shear stresses on the top and bottom surfaces of the slab are very small as compared with the lithostatic stress. This is compatible with the low effective mantle wedge viscosity predicted by thermal modeling ([Wada et al., 2008](#)). By modeling force and torque balance and intraplate stresses of the JDF plate before subduction, [Wang et al. \(1997\)](#) already concluded that the strike-parallel mantle resistance (discussed in the [Nootka Shear and Strike-Parallel Mantle Resistance to Slab Motion](#) section) is small, and by inference the total mantle resistance is also small. It is the updip component of this small mantle resistance that balances most of the slab pull. This means that the slab pull itself must also be very small, consistent with the JDF slab being young, warm, and thus buoyant. We think a subtle balance between the two small forces, slab pull and mantle resistance, controls deviatoric stresses in most of the JDF slab.

Overall, deviatoric stresses in the JDF plate seem to be small except for the northernmost and southernmost areas (region A and shallow part of region D). This view is consistent with the overall low intraslab seismicity in Cascadia as compared with most other subduction zones in the world. Because the deviatoric stresses are small, they vary readily in response to small spatial changes in tectonic forces. For example, a slight decrease in the mantle resistance will result in a net slab pull, causing downdip-tension earthquakes, and a slight increase will diminish the net slab pull. According to

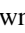
this view, the near lack of intraslab seismicity in most of southern Cascadia is merely a locally but slightly amplified expression of the overall low intraslab stresses in this subduction zone.

A slightly stronger mantle resistance due to a slightly higher mantle viscosity can make the net slab pull in most of southern Cascadia very small. There are some candidate mechanisms for the variation of mantle viscosity along the Cascadia subduction zone. For example, the generally cooler subducting plate may cause a greater increase in effective mantle viscosity than in slab pull beneath Oregon, and a proposed mantle plume may decrease mantle viscosity in the north ([Xue and Allen, 2007](#)). It is beyond our present knowledge to speculate on specific mechanisms that might cause variations of mantle viscosity, but we wish to point out that along-strike variations of physical properties of the mantle are commonly inferred from seismic imaging of subduction zones and therefore should not be a surprise for Cascadia.

Conclusion

The state of stress in the subducting JDF slab inferred by inverting focal mechanism solutions for most of northern Cascadia is slab-normal compression and downdip-tension. It is most likely caused by a small net slab pull. An exception to this is the northernmost area near the NFZ, where the shallow part of the slab experiences large east–west tension. We hypothesize that the tension is a combined effect of the margin-parallel mantle resistance to the obliquely subducting slab and the NFZ shear. Near the MTJ, the corner of the Pacific plate pushes against the southernmost part of the subducting plate, inducing strong north–south compression. The north–south compression is observed only in the shallow part of the slab (< 20 km depth); stresses in the deeper part of the slab are controlled primarily by the net slab pull, similar to northern Cascadia. Stresses causing earthquakes in most of the JDF slab appear to be small deviations from the lithostatic state. The near lack of intraslab earthquakes in most of southern Cascadia is thus merely a more pronounced expression of the state of low stress in the JDF slab.

Data and Resources

The Oregon State University database of moment-tensor solutions was searched by using <http://quakes.oce.orst.edu/moment-tensor> (last accessed on 28 October 2008). The PNSN and NEIC databases of first-motion focal mechanism solutions were searched by using www.pnsn.org/CATDAT/focal.html (last accessed on 28 October 2008) and <http://neic.usgs.gov/neis/sopar> (last accessed on 1 November 2008), respectively. The rest of the data used in stress inversion are from published sources listed in the references. Focal mechanism data used in stress inversion and in [Figure 3a](#) are tabulated  in the electronic supplement to this article. The moment-tensor solutions for earthquakes in the NFZ and

Explorer plate area shown in Figure 9 were provided by Ristau (2004) and H. Kao (2008, personal communication).

Statistical analysis was performed by using the R software (<http://www.r-project.org/>). The code for the Bayesian inversion was obtained through personal communication with J. Townend. Figures were generated with the help of the Generic Mapping Tool (Wessel and Smith, 1995).

Acknowledgments

We thank R. Arnold and J. Townend for their guidance in using their Bayesian stress inversion method, A. J. Michael for his guidance in using his linear inversion method, and H. Kao for providing moment tensor solutions. The paper benefitted from comments from two anonymous reviewers and associate editor F. Pollitz. This research was partially supported by the Natural Sciences and Engineering Research Council of Canada. Geological Survey of Canada contribution 20090087.

References

- Arnold, R., and J. Townend (2007). A Bayesian approach to estimating tectonic stress from seismological data, *Geophys. J. Int.* **170**, 1336–1356.
- Bolton, M. K. (2003). Juan de Fuca plate seismicity at the northern end of the Cascadia subduction zone, *M.Sc. Thesis*, University of Victoria, British Columbia, Canada.
- Braunmiller, J., and J. Nábělek (2002). Seismotectonics of the Explorer region, *J. Geophys. Res.* **107**, no. B10, 2208, doi [10.1029/2001JB000220](https://doi.org/10.1029/2001JB000220).
- Calvert, A. J. (2004). Seismic reflection imaging of two megathrust shear zones in the northern Cascadia subduction zone, *Nature* **428**, 163–167.
- Cassidy, J. F., and F. Waldhauser (2003). Evidence for both crustal and mantle earthquakes in the subducting Juan de Fuca plate, *Geophys. Res. Lett.* **30**, doi [10.1029/2002GL015511](https://doi.org/10.1029/2002GL015511).
- Chiao, L. Y., and K. C. Creager (2002). Geometry and membrane deformation rate of the subducting Cascadia slab, in *The Cascadia subduction zone and related subduction system—Seismic structure, intraslab earthquakes and processes, and earthquake hazards*, S. Kirby, K. Wang, and S. Dunlop (Editors), *U.S. Geol. Surv. Open-File Rept. 02-328*, 47–54.
- DeMets, C., R. G. Gordon, D. F. Argus, and S. Stein (1990). Current plate motions, *Geophys. J. Int.* **101**, 423–478.
- DeMets, D., R. G. Gordon, D. F. Argus, and S. Stein (1994). Effect of recent revision to the geomagnetic reversal time scale on estimates of current plate motions, *Geophys. Res. Lett.* **21**, 2191–2194.
- Gephart, J. W., and D. W. Forsyth (1984). An improved method for determining regional stress tensor using earthquake focal mechanism data: Application to the San Fernando earthquake sequence, *J. Geophys. Res.* **89**, 9305–9320.
- Gripp, A. E., and R. G. Gordon (2002). Young tracks of hotspots and current plate velocities, *Geophys. J. Int.* **150**, 321–361.
- Hacker, B. R., S. M. Peacock, G. A. Abers, and S. D. Holloway (2003). Subduction factory 2. Are intermediate-depth earthquakes in subducting slabs linked to metamorphic dehydration reactions? *J. Geophys. Res.* **108**, 2030, doi [10.1029/2001JB001129](https://doi.org/10.1029/2001JB001129).
- Hardebeck, J. L., and E. Hauksson (2001). Stress orientations obtained from earthquake focal mechanisms: What are appropriate uncertainty estimates? *Bull. Seismol. Soc. Am.* **91**, 250–262.
- Kao, H., K. Wang, R.-Y. Chen, I. Wada, J. He, and S. D. Malone (2008). Identifying rupture plane of the 2001 Nisqually, Washington, earthquake, *Bull. Seismol. Soc. Am.* **98**, 1546–1558.
- Kastrup, U., M. L. Zoback, N. Deichmann, K. F. Evans, D. Giardini, and A. J. Michael (2004). Stress field variations in the Swiss Alps and the northern Alpine foreland derived from inversion of fault plane solutions, *J. Geophys. Res.* **109**, doi [10.1029/2003JB002550](https://doi.org/10.1029/2003JB002550).
- Kirby, S. H., E. R. Engdahl, and R. Denlinger (1996). Intermediate-depth intraslab earthquakes and arc volcanism as physical expressions of crustal and uppermost mantle metamorphism in subducting slabs, in *Subduction: Top to Bottom*, G. E. Bebout, D. W. Scholl, S. H. Kirby, and J. P. Platt (Editors), American Geophysical Monograph 96, Washington, D.C., 195–214.
- Lamb, S. (2006). Shear stresses on megathrusts: Implications for mountain building behind subduction zones, *J. Geophys. Res.* **111**, B07401, doi [10.1029/2005JB003916](https://doi.org/10.1029/2005JB003916).
- Ma, L., R. Crosson, and R. Ludwin (1996). Western Washington earthquake focal mechanisms and their relationship to regional tectonic stress, in *Assessing earthquake hazards and reducing risk in the Pacific Northwest I*, A. M. Rogers, T. J. Walsh, W. J. Kocheleman, and G. R. Priest (Editors), *U.S. Geol. Surv. Profess. Pap. 1560*, 257–283.
- McCaffrey, R. A., I. Qamar, R. W. King, R. Wells, G. Khazaradze, C. A. Williams, C. W. Stevens, J. J. Vollick, and P. C. Zwick (2007). Fault locking, block rotation and crustal deformation in the Pacific Northwest, *Geophys. J. Int.* **169**, 1315–1340.
- McCrory, P. A., J. L. Blair, D. H. Oppenheimer, and S. R. Walter (2004). Depth to the Juan de Fuca slab beneath the Cascadia subduction margin: A 3-D model for sorting earthquakes, *U.S. Geol. Surv. Data Ser. DS-91*, 1 CD-ROM.
- McKenzie, D. (1969). The relationship between fault plane solutions for earthquakes and the directions of the principal stresses, *Bull. Seismol. Soc. Am.* **59**, 591–601.
- Medema, G. F., R. S. Crosson, and K. C. Creager (2004). Evidence of two source mechanisms for Cascadia intraslab seismicity from an anomalous secondary *P* arrival, *Eos Trans. AGU* **85**, no. 47, Fall Meet. Suppl., Abstract S53A-0186.
- Michael, A. J. (1984). Determination of stress from slip data: Faults and folds, *J. Geophys. Res.* **89**, 11,517–11,526.
- Michael, A. J. (1987). Use of focal mechanisms to determine stress: A case study, *J. Geophys. Res.* **92**, 357–368.
- Michaelson, C. A., and C. S. Weaver (1986). Upper mantle structure from teleseismic *P* wave arrivals in Washington and northern Oregon, *J. Geophys. Res.* **91**, 2077–2094.
- Reasenber, P., and D. Oppenheimer (1985). FPFIT, FPLOT, and FPPAGE: FORTRAN computer programs for calculating and displaying earthquake fault-plane solutions, *U.S. Geol. Surv. Open-File Rept. 85-739*.
- Riddihough, R. (1984). Recent movements of the Juan de Fuca plate system, *J. Geophys. Res.* **89**, 6980–6994.
- Riddihough, R. P., and R. D. Hyndman (1989). Queen Charlotte Islands margin, in *The Geology of North America, vol. N, The Eastern Pacific Ocean and Hawaii*, E. L. Winterer, D. M. Hussong, and R. W. Decker (Editors), Geol. Soc. of Am., Boulder, Colorado, 403–411.
- Ristau, J. (2004). Seismotectonics of Western Canada from regional moment tensor analysis, *Ph.D. Thesis*, University of Victoria, British Columbia, Canada.
- Rohr, K. M. M., and K. P. Furlong (1995). Ephemeral plate tectonics at the Queen Charlotte triple junction, *Geology* **23**, 1035–1038.
- Rondenay, S., G. A. Abers, and P. E. van Keken (2008). Seismic imaging of subduction zone metamorphism, *Geology* **36**, 275–278.
- Roth, J. B., M. J. Fouch, D. E. James, and R. W. Carlson (2008). Three-dimensional seismic velocity structure of the northwestern United States, *Geophys. Res. Lett.* **35**, L15304, doi [10.1029/2008GL034669](https://doi.org/10.1029/2008GL034669).
- Sandiford, M., D. Coblenz, and W. P. Schellart (2005). Evaluating slab-plate coupling in the Indo-Australian plate, *Geology* **33**, 113–116.
- Schellart, W. P. (2004). Quantifying the net slab pull force as a driving mechanism for plate tectonics, *Geophys. Res. Lett.* **31**, L07611, doi [10.1029/2004GL019528](https://doi.org/10.1029/2004GL019528).
- Sigloch, K., N. McQuarrie, and G. Nolet (2008). Two-stage subduction history under North America inferred from multiple-frequency tomography, *Nature Geoscience* **1**, 458–462.
- ten Brink, U. S., N. Shimizu, and P. C. Molzer (1999). Plate deformation at depth under northern California: Slab gap or stretched slab? *Tectonics* **18**, 1084–1098.

- Wada, I., K. Wang, J. He, and R. D. Hyndman (2008). Weakening of the subduction interface and its effects on surface heat flow, slab dehydration, and mantle wedge serpentinization, *J. Geophys. Res.* **113**, B04402, doi [10.1029/2007JB005190](https://doi.org/10.1029/2007JB005190).
- Wang, K., and J. He (1999). Mechanics of low-stress forearcs: Nankai and Cascadia, *J. Geophys. Res.* **104**, 15,191–15,205.
- Wang, K., and G. C. Rogers (1994). An explanation for the double seismic layers north of the Mendocino triple junction, *Geophys. Res. Lett.* **21**, 121–124.
- Wang, K., J. He, and E. E. Davis (1997). Transform push, oblique subduction resistance, and intraplate stress of the Juan de Fuca plate, *J. Geophys. Res.* **102**, 661–674.
- Wang, K., J. Cassidy, I. Wada, and A. J. Smith (2004). Effects of metamorphic crustal densification on earthquake size in warm slabs, *Geophys. Res. Lett.* **31**, L01605, doi [10.1029/2003GL018644](https://doi.org/10.1029/2003GL018644).
- Wang, K., I. Wada, and Y. Ishikawa (2004). Stresses in the subducting slab beneath Southwest Japan and relation with plate geometry, tectonic forces, slab dehydration, and damaging earthquakes, *J. Geophys. Res.* **109**, B08304, doi [10.1029/2003JB002888](https://doi.org/10.1029/2003JB002888).
- Wang, K., R. Wells, S. Mazzotti, R. D. Hyndman, and T. Sagiya (2003). A revised dislocation model of interseismic deformation of the Cascadia subduction zone, *J. Geophys. Res.* **108**, 2026, doi [10.1029/2001JB001227](https://doi.org/10.1029/2001JB001227).
- Wessel, P., and W. H. F. Smith (1995). New version of the Generic Mapping Tools released, *Eos Trans. AGU* **76**, 329.
- Wilson, D. S. (1988). Tectonic history of the Juan de Fuca Ridge over the last 40 million years, *J. Geophys. Res.* **93**, 11,863–11,876.
- Wilson, D. S. (1993). Confidence intervals for motion and deformation of the Juan de Fuca plate, *J. Geophys. Res.* **98**, 16,053–16,071.
- Wong, I. G. (2005). Low potential for large intraslab earthquakes in the central Cascadia subduction zone, *Bull. Seismol. Soc. Am.* **95**, 1880–1902.
- Xue, M., and R. M. Allen (2007). The fate of the Juan de Fuca plate: Implications for a Yellowstone plume head, *Earth Planet. Sci. Lett.* **264**, 266–276.

School of Earth and Ocean Sciences
University of Victoria
3800 Finnerty Road, Victoria
British Columbia V8W 3V6, Canada
(I.W.)

Geological Survey of Canada
Pacific Geoscience Centre
9860 West Saanich Road, Sidney
British Columbia V8L 4B2, Canada
(S.M., K.W.)

Manuscript received 30 October 2009